

Non-halogenated Imidazolium and Phosphonium-based Surface-Active Ionic Liquids as Electrolytes for Supercapacitors

Preeti Jain^{a*}, Oleg N. Antzutkin^{ab}

^a*Chemistry of Interfaces, Luleå University of Technology, SE-97 187, Luleå, Sweden*

^b*Department of Physics, Warwick University, CV4 7AL, Coventry, United Kingdom*

*E-mails: preeti.9jain@gmail.se; Oleg.Antzutkin@itu.se

Abstract

We report a comparative analysis of three novel non-halogenated surface-active ionic liquids (SAILs), which consist of a surface-active anion, 2-ethylhexyl sulfate ([EHS]⁻), and phosphonium or imidazolium cations: tetrabutylphosphonium ([P_{4,4,4,4}]⁺), trihexyl(tetradecyl)phosphonium ([P_{6,6,6,14}]⁺), and 1-methyl-3-hexylimidazolium ([C₆C₁Im]⁺). We explored thermal properties (degradation, melting and crystallisation temperatures) of these novel SAILs and their electrochemical properties (ionic conductivity and electrochemical potential window, ECW). These SAILs were tested as electrolytes in a multi-walled carbon nanotubes (MWCNTs)-based supercapacitor at various temperatures from 253 to 373 K and their electrochemical performance as a function of temperature was compared. We found that the supercapacitor cell with [C₆C₁Im][EHS] as an electrolyte has shown a higher specific capacitance (C_{elec} in F g⁻¹), a higher energy density (E in W h kg⁻¹), and a higher power density (P in kW kg⁻¹) as compared to the other studied SAILs, [P_{4,4,4,4}][EHS], [P_{6,6,6,14}][EHS] and [N_{8,8,8,8}][EHS] (from previous our study) at a temperature range from 253 to 373 K. The supercapacitor with an MWCNT-based electrode and [C₆C₁Im][EHS], [P_{4,4,4,4}][EHS] and [P_{6,6,6,14}][EHS] as electrolytes showed a specific capacitance of 148, 90 and 47 F g⁻¹ (at the scan rate of 2 mV s⁻¹) with an energy density of 82, 50 and 26 W h kg⁻¹ (at 2 mV s⁻¹), respectively, all at 298 K. For latter three SAILs, the temperature effect can be seen by a two to three-fold increase in the specific capacitance of the cell and the energy density values: 290, 198 and 114 F g⁻¹ (at 2 mV s⁻¹) and 161, 110 and 63 Wh kg⁻¹ (at 2 mV s⁻¹), respectively, at 373 K. The solution resistance (R_s), charge transfer resistance (R_{ct}), and equivalent series resistance (ESR) also decreased with an increase in temperature for all SAILs in this study. These new SAILs can potentially be used for high-temperature electrochemical applications, such as supercapacitors for high energy storage due to a reasonably high specific capacitance and enhanced energy and power density, and wider ECWs as compared to molecular organic and

aqueous electrolytes. Specifically, [C₆C₁Im][EHS] and [P_{4,4,4,4}][EHS], are the best candidates among other “EHS”-based SAILs in this and our previous study, as electrolytes in supercapacitors.

Keywords: Non-halogenated ionic liquids; Surface-active ionic liquids; Conductivity; Specific capacitance; Electric energy density; Electric power density; MWCNT-based supercapacitors

Introduction

Ionic liquids (ILs) have been the topic of immense interest as an electrolyte for energy storage devices due to their unique properties, such as low volatility, non-flammability, and high thermal and chemical stability, along with a high electrochemical stability at ambient and elevated temperatures.¹⁻⁶ Among many different classes of ionic liquids, quaternary aprotic room temperature ILs (RTILs) are special due to their high hydrophobicity and thermal-electrochemical stability. The most common quaternary ionic liquids consist of ammonium or phosphonium cations with non-branched alkyl side chains of different length. Usually, these RTILs are highly viscous with a low electrical conductivity at room temperature due to a large molecular size of their cations and a low ionicity, because of formation of hydrophobically aggregated nanoscale domains.⁷⁻¹¹ However, the challenge with a high viscosity can be tackled with fine-tuning of chemical moieties in both cationic and anionic components of ILs, for example, by changing lengths and branching of alkyl groups, to make RTILs more useful as electrolytes in energy storage devices. Few studies on ammonium and phosphonium cation-based ILs with common anions like bis(trifluoromethanesulfonyl)imide, [NTf₂]⁻, or bis(fluorosulfonyl)imide, [FSI]⁻, have shown a promising performance of these halogenated RTILs as electrolytes with a low viscosity and a three-four fold larger electrochemical potential window (ECW) as compared to ECWs of molecular organic and standard KOH(aq) and H₂SO₄(aq) based electrolytes.¹² However, due to high costs and the presence of halides, the use of halogenated RTILs is rather limited as electrolytes in supercapacitors.¹³⁻¹⁵ Halogen containing anions are prone to hydrolysis giving rise to halide anions. The halides such as F⁻ and Br⁻ may result in dealkylation reactions of phosphonium, ammonium and imidazolium cations and do reduce the electrochemical stability of ionic liquids by their anodic oxidation at a rather low electrical potential.²

The use of ILs in supercapacitors as electrolytes or components of electrolytes is a topic of research interest.^{12, 16, 17} Supercapacitors have already emerged as electrical energy storage devices and have drawn a significant attention of the scientific community due to their high energy and power density, safety (a low risk of explosion at high temperatures as happens for organic electrolytes)¹⁸ and long-term recyclability and stability. The efficiency of the capacitor primarily depends on the electrode material used, and the operating potential voltage determined by the ECW of the electrolyte. Intriguingly, ionic liquids exhibit interesting properties near charged surfaces that determine the performance of energy devices. In fact, recent experimental and theoretical evidence has shown the formation of an electric double layer (EDL) structure in capacitors near charged electrodes.^{16, 19-21} ILs in the EDL behave differently when compared with aqueous and organic (molecular) electrolytes due to specific ion ordering in ionic liquids.²²⁻²⁴ Mao et al. have recently explored the electro-capacitive characteristics and EDL nanostructures of surface-active ILs (SAILs).¹⁶ SAILs can be considered as an important class of ILs since they form stable nanostructures on the hydrophobic electrode surfaces. SAILs are amphiphilic molecules with polar head groups and hydrophobic tails that enable them to form stable nanostructures, unlike non-amphiphilic ILs (NAILs). Nanostructures formed by NAILs are typically smaller and less stable (less ordered) than those formed by SAILs.^{16, 19, 25} Therefore, SAILs can be used as electrolytes or components of electrolytes in supercapacitors and batteries to operate under a wider range of temperatures.^{12, 16} A more thorough investigation of SAILs may increase the traditional understanding of ILs in electrochemistry. There is very little known about the SAILs and, to the best of our knowledge, few studies performed on this new class of ionic liquids, which comprise a surface-active anion like 1,4-bis(2-ethylhexoxy)-1,4-dioxobutane-2-sulfonate (AOT)¹⁶ and 2-ethylhexyl sulfate¹² as electrolytes or as components of electrolytes in supercapacitors.

While turning to their practical applications, the applied voltage and operating temperature range are of great importance for the construction of supercapacitor devices. High viscosity and low ionic conductivity are typically responsible for an increase in the internal resistance in capacitors. The chemical structure of the ions affects the formation of the electrical double layer (EDL), which may also deteriorate the capacitance of supercapacitors. Therefore, to increase the performance of supercapacitors, in particular, to enhance their energy and power density, a wide operating ECW and a wide operating temperature interval of electrolytes is required. In addition, an appropriate selection of the chemical structure of the constituent ions

is desired to enhance the interaction between the electrolyte and electrode surfaces to facilitate the formation of stable EDLs and to increase the specific capacitance of the device. Temperature-dependent electrode-electrolyte interactions combined with a wide operating ECW are important parameters to consider to augment the double-layer capacitance of the supercapacitors.

The present study is a continuation of our recent work on a novel SAIL, namely, tetraalkylammonium 2-ethylhexyl sulfate, $[N_{8,8,8,8}][EHS]$.¹² Here, we explore novel SAILs, which contain the same surface-active anion, 2-ethylhexyl sulfate ($[EHS]^-$) and a range of different phosphonium and imidazolium cations, such as tetrabutylphosphonium ($[P_{4,4,4,4}]^+$), trihexyl(tetradecyl)phosphonium ($[P_{6,6,6,14}]^+$) and 1-methyl-3-hexylimidazolium ($[C_6C_1Im]^+$) as potential electrolytes in supercapacitors. $[EHS]^-$ is an amphiphilic anion comprising of a polar and charged sulfate group and a non-polar and branched alkyl group with eight aliphatic carbons (see **Figure 1**). Due to these distinct polar and non-polar domains, $[EHS]$ -based ILs can self-assemble into nanostructures.^{26, 27} Moreover, non-halogenated and surface-active alkylsulfate anions are environmentally benign, cheap and already widely used in soaps, shampoo and detergents. These non-halogenated ILs are non-toxic and more readily biodegradable compared to the other, unfortunately, already widely used in electrochemical applications, halide-containing ionic liquids. The latter ILs are metal halide complexes with $[PF_6]^-$ (widely used as $Li[PF_6]$ in lithium ion batteries (LIBs)), $[BF_4]^-$, $[NTf_2]^-$ and $[OTf]^-$, which are moisture-sensitive, prone to hydrolysis, corrosive to metals and, which require special expensive lines in production.^{2, 28-30}

In this work, we report on the performance of neat $[P_{4,4,4,4}][EHS]$, $[P_{6,6,6,14}][EHS]$ and $[C_6C_1Im][EHS]$ as electrolytes in capacitors with multi-walled carbon nanotubes (MWCNT) as an electrode material tested in different electrochemical experiments at different temperatures. MWCNT were chosen in combination with SAILs, because of their specific properties, such as their high electrical conductivity, distinctive charge transfer capability, high electrochemical stability, high electrolyte accessibility, and double-layer capacitor behaviour.³¹⁻³⁴ The electrochemical performance of studied here SAILs as electrolytes is also compared with that of the previously reported SAIL, $[N_{8,8,8,8}][EHS]$, and its binary 50 wt% mixture with acetonitrile and with 6 M KOH(aq) as electrolytes in MWCNT-based supercapacitors in the same temperature range.¹² We showed that using SAILs as electrolytes, one could achieve improved specific capacitance and a high energy and power density,

particularly, at elevated temperatures up to 373 K and with a good cycling stability of the MWCNT-based supercapacitor.

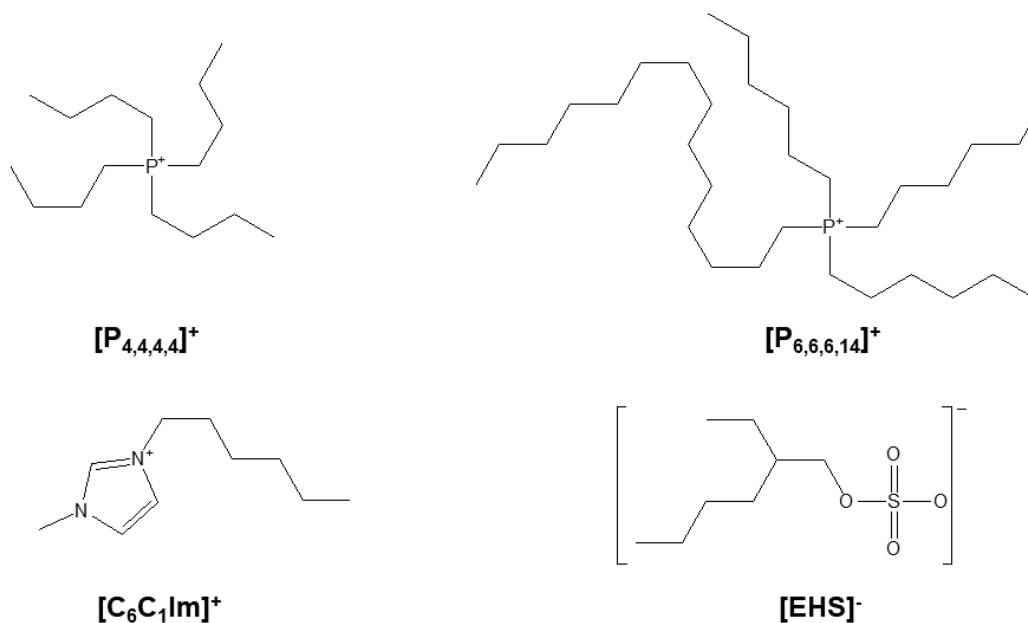


Figure 1. Chemical structures of tetrabutylphosphonium, $[P_{4,4,4,4}]^+$, trihexyl(tetradecyl)phosphonium, $[P_{6,6,6,14}]^+$, and 1-methyl-3-hexylimidazolium, $[C_6C_1Im]^+$, cations and the 2-ethylhexyl sulfate, $[EHS]^-$, anion.

Experimental Section

Chemicals and Materials

Tetrabutylphosphonium chloride solution, $[P_{4,4,4,4}][Cl]$ (50% solution in water) was purchased from CYTEC, trihexyl(tetradecyl)phosphonium chloride, $[P_{6,6,6,14}][Cl]$, and 1-methyl-3-hexylimidazolium bromide, $[C_6C_1Im][Br]$, were purchased from Solvionic. Sodium 2-ethylhexyl sulfate (50% solution in water) was purchased from Sigma-Aldrich. Dichloromethane from VWR was used as received. All the materials were not additionally purified before the metathesis reactions.

For the electrode material, multi-walled carbon nanotubes (MWCNTs), activated carbon, and polyvinyl alcohol (PVA) were purchased from Sigma-Aldrich and used as received without further purification.

Synthesis and Characterisation of SAILs

The final product, ([P_{4,4,4,4}][EHS], [P_{6,6,6,14}][EHS] and [C₆C₁Im][EHS]) was prepared by the ion exchange (metathesis) reactions between a starting salt ([P_{4,4,4,4}][Cl], [P_{6,6,6,14}][Cl] and [C₆C₁Im][Br], respectively) and [Na][EHS] in dichloromethane (DCM) at room temperature. The corresponding SAIL was prepared by adding the sodium salt of [EHS]⁻ (1.1 mmol) to the stirred solution of a starting chloride or bromide salt of cations used in this study (1 mmol) in DCM. The reaction mixture was stirred for 48 hours at ambient pressure (ca. 1 bar) and at room temperature (ca. 295 K). To remove the excess of the reagent ([Na][EHS] salt) from the final product, the reaction mixture was then washed with distilled water three times. The excess water and DCM was removed using a rotary evaporator. To further remove traces of DCM and water, the final products (SAILs) were kept in a vacuum oven at 353 K for 4 days. Both SAILs identity and purity were checked by solution ¹H, ¹³C and ³¹P (for phosphonium-based SAILs) NMR spectroscopy. Residual content of Br⁻, Cl⁻ and Na⁺ ions (recommended levels of <500 ppm) was analysed using Inductive Coupled Plasma Atomic Emission Spectroscopy (ICP-AES) by ALS Scandinavia, Luleå. Solution NMR spectra (see **Figures S1-S8**) and results of the elemental analysis (see **Table S1**) are provided in the Electronic Supplementary Information (ESI).

Nuclear Magnetic Resonance (NMR) Spectroscopy

Solution ¹H, ¹³C and ³¹P NMR spectra of SAILs (in CDCl₃ with 0.03% v/v TMS) were obtained using a 400 MHz Bruker Avance III NMR spectrometer (Bruker BioSpin AG, Fällanden, Switzerland) with an Aeon 9.4 T zero-helium boil-off superconducting magnet and 10 or 5 mm probes for liquids. Working frequencies were 400.27 MHz for ¹H, 100.64 MHz for ¹³C and 162.000 MHz for ³¹P. Proton decoupling pulse sequence WALTZ-16 was used for ¹³C NMR. For ¹H 90°-pulse duration and the recycling delay were 9 μs and 1 s, respectively. For ¹³C, 30°-pulse duration of 9 μs and a recycling delay of 3 s were used to minimize the signal saturation effects due to the longer T₁ relaxation time of ¹³C sites. For the same reason, ³¹P 30°-pulse duration and the recycling delay were 25 μs and 2 s, respectively. Bruker “Topspin-3.5” software was used for NMR data processing.

Thermogravimetric Analysis (TGA)

TGA was performed using a Perkin Elmer TGA 8000 instrument with about 3 mg of a SAIL sample from 303 K to 973 K at a rate of 10 K min⁻¹ under nitrogen gas flow of 20 mL min⁻¹.

Differential Scanning Calorimeter (DSC)

A Perkin Elmer DSC 6000 instrument was used to measure melting, crystallisation and glass transition temperatures for all SAILs in this study. For these experiments, about 4 mg of a SAIL sample was packed in an aluminium pan. Heating and cooling DSC scans were recorded from 213 to 373 K at a rate of 10 K min⁻¹ for all samples. To maintain a dry environment inside the sample chamber, nitrogen gas was supplied at a flow of 20 mL min⁻¹.

Pellet Formation

A stainless-steel pellet die was used for pellet formation. The electrode used for the current study mainly contains the MWCNTs, activated carbon, and PVA as a binder in a 7:2:1 ratio by weight, respectively. A powder composed of these three compounds was carefully mixed using a pestle and a mortar. Then pellets were pressed at varying pressures (300-1000 kPa) by a manual press. Pellets were 10 mm in diameter. The sample weight of a pellet was ca. 10 mg. Glass microfiber Whatman filter paper was used as a separator.

Electrochemical Measurements

All electrochemical measurements were performed using a Metrohm Autolab (PGSTAT302N) electrochemical workstation, with the FRA32M module for impedance measurements. Conductivity of electrolytes used in this study (neat SAILs: [P_{4,4,4,4}][EHS], [P_{6,6,6,14}][EHS] and [C₆C₁Im][EHS]) was measured using ca. 70 μL of a SAIL in a TSC 70 closed cell (RHD instruments) in the temperature range between 253 and 373 K. The supercapacitor measurements were carried out in a TSC battery cell, which was mounted on the Microcell HC stand with a Peltier element to control the sample temperature with a precision of ±1 K in a temperature range from 269 to 373 K. Prior to each experiment, two electrodes were polished using a Kemet diamond paste (0.25 μm). For data processing, Nova 2.1.4 software was used. ECWs for the studied SAILs were determined by cyclic voltammetry (CV) at 293 K using a two-electrode cell assembly with a glassy carbon working electrode and a platinum cup as the counter electrode at the scan rate 100 mV s⁻¹. This two-electrode cell assembly was also used to measure the ionic conductivity by electrochemical impedance spectroscopy (EIS). All EIS experiments were performed in the frequency range from 0.01 Hz to 1 MHz with an alternating current (AC) amplitude of 10 mV. The cell was thermally equilibrated prior to each measurement for at least 10 min.

An MWCNT-supercapacitor device contained two pellets with a filter paper sandwiched between them as a separator (see **Figure 2**). The filter paper was kept in a SAIL electrolyte for 24 hours before measurements were taken. The cell consists of nickel-plated copper lower and

upper current collectors with an average contact area of 8 mm in diameter each (the TSC battery cell). Therefore, an active surface area of pellets was also 8 mm in diameter. A glass microfiber Whatman filter paper of 12 mm in diameter was used as a separator. The cell was packed with a screw cap, and the contact pressure was adjusted to 40.7 kPa using a gold-plated spring with a spring constant of 2.3 N mm⁻¹.

The electrochemical performance of the supercapacitor was measured in a two-electrode cell assembly at various temperatures. The electrochemical measurements were carried out using a TSC battery cell assembly as shown in **Figure 2**.

In the electrochemical tests, the supercapacitor was activated by CV at a lower scan rate, 50 cycles at 5 mV s⁻¹ at 313 K for [P_{4,4,4,4}][EHS] (see **Figure S9** in the ESI) and 25 cycles at 5 mV s⁻¹ at 333 K for [C₆C₁Im][EHS] (see **Figure S10** in the ESI). Later, electrochemical impedance spectroscopic (EIS) measurements were performed followed by CVs at different scan rates and GCD experiments. At each temperature before recording CVs at different scan rates, 5 cycles were recorded at 2 mV s⁻¹ for further activation of the electrode. Thereafter, CVs were recorded at different scan rates (from 2 to 100 mV s⁻¹) and at different temperatures interrupted by EIS measurements at each temperature. GCD tests were performed in the electric potential range from -2 to +2 V for [P_{4,4,4,4}][EHS] and [C₆C₁Im][EHS] and from -2.5 to 2.5 V for [P_{6,6,6,14}][EHS] at different current densities: 0.07, 0.11, and 0.14 A g⁻¹. The electrochemical measurements were performed for all the studied SAILs in the electric potential range from -2 to +2 V (ECW = 4V). Additionally, the performance of supercapacitor cells was also explored in the electric potential range from -2.5 to +2.5 V (ECW = 5V) for [P_{6,6,6,14}][EHS] (at 298, 313, 333 and 373 K) and [P_{4,4,4,4}][EHS] (at 298 and 373 K)

The specific capacitance of the material (C_{elec} in F g⁻¹), the energy density (E in W h kg⁻¹) and the power density (P in kW kg⁻¹) of the supercapacitor cell were calculated from the CV curves¹⁶ using Eqs. (1), (2) and (3), respectively as given below:

$$C_{elec} = 4 \frac{\int IdV}{m \left(\frac{dV}{dt} \right)} \quad (1)$$

$$E = \frac{C_{sp} V^2}{2} \times \frac{1000}{3600} \quad (2)$$

$$P = \frac{E \left(\frac{dV}{dt} \right)}{V} \times \frac{3600}{1000} \quad (3)$$

where I is current (in A), dV/dt is a scan rate (in $V\ s^{-1}$), m is the total weight of the electrode material (in g), V is the applied cell potential (in V), $\int IdV$ are total areas (both positive and negative but added as modulus) identified by $I(V)$ curves in the CV plots, and C_{sp} is the capacitance of the supercapacitor device ($C_{sp} = C_{elec}/4$).

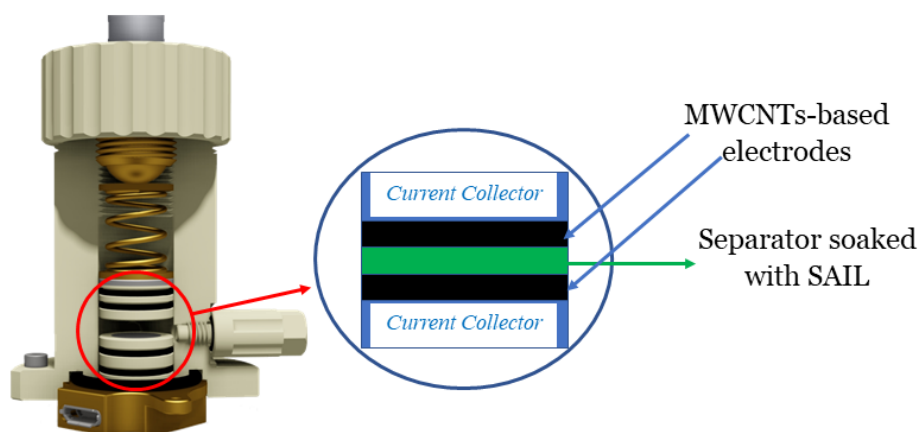


Figure 2. A setup used in electrochemical measurements for a supercapacitor cell with MWCNT-based electrodes and neat $[P_{4,4,4,4}][EHS]$, $[C_6C_1Im][EHS]$ and $[P_{6,6,6,14}][EHS]$ as electrolytes. The supercapacitor is yet not placed in the setup.

Results and Discussion

Electrical Conductivity and Electrochemical Potential Window of SAILs

Electrical conductivity in aprotic ILs originates predominantly from the intrinsic mobility of cations and anions. In the present study on SAILs containing the same 2-ethylhexyl sulfate anion but different cations, we explore major structural impacts of cations on the electrical conductivity and electrochemical stability of these SAILs. The ionic conductivity of neat SAILs, $[C_6C_1Im][EHS]$, $[P_{4,4,4,4}][EHS]$ and $[P_{6,6,6,14}][EHS]$ was measured using GC-electrodes in the temperature range from 253 to 373 K. Measurements at each temperature point were performed in duplicate, first, during sample heating and, then, during cooling. The conductivity data points obtained during sample heating and cooling were close to each other (see **Figure 3**). The electrical conductivity of $[C_6C_1Im][EHS]$ was found to be higher compared to that of $[P_{4,4,4,4}][EHS]$ and $[P_{6,6,6,14}][EHS]$ in the whole temperature range studied. For example, at 298 K, conductivities are 73.19, 18.74 and 5.44 $\mu S\ cm^{-1}$ for $[C_6C_1Im][EHS]$, $[P_{4,4,4,4}][EHS]$ and $[P_{6,6,6,14}][EHS]$, respectively, and increased ca. 20-40 fold for these three SAILs at 373 K, up

to 1.62, 0.68 and 0.15 mS cm⁻¹, respectively. The electrical conductivity in ionic liquids is mainly dependent on the ionicity (the number of mobile ions available in the system) and viscosity of ILs. Therefore, a significant difference in the electrical conductivity of the three SAILs in this study, particularly, at near-room temperatures can be explained by differences in viscosity and in formation of ionic complexes due to specific electrostatic and van der Waals interactions leading to aggregation and ion-pairing. These factors result in both a low ionicity and a low ionic mobility, thus, to a low electrical conductivity in SAILs. On the other hand, upon an increase in temperature, viscosity of ILs decreases almost exponentially. Therefore, both the ion mobility and the electrical conductivity do increase abruptly with temperature. Despite a low electrical conductivity at ambient temperatures, this class of SAILs can yet be considered as a good electrolyte for supercapacitors, when compared to organic- and aqueous-based electrolytes due to a two-four fold larger ECWs of SAILs (see **Figure 4**). The ECW of an electrolyte plays a crucial role in the supercapacitors, because the electric energy density of these devices depends on the square of the operating voltage (see Eq. (2)). Therefore, a larger amount of energy can be stored in these devices with SAILs as electrolytes compared to “standard” organic- and aqueous-based electrolytes.

CVs recorded at the scan rate of 100 mV s⁻¹ and at 298 K for different electric potential windows revealed the electrochemical stability (no redox peaks in the CV curves) with applied electric potential from +2 to -2 V for phosphonium-based SAILs, [P_{6,6,6,14}][EHS] and [P_{4,4,4,4}][EHS]. Therefore, these SAILs can be used as electrolytes in the electric potential range from -2 to +2 V. On the other hand, two small peaks around -0.5 V and +1.3 V were observed in the CV curves for [C₆C₁Im][EHS] (see **Figure 4**). This might be because of the carbene formation in neat alkylsulfate-based ILs as reported previously.³⁵ [C₆C₁Im][EHS] also shows some redox peaks in the supercapacitor device at elevated temperatures (see Figure S12 in ESI). These processes are, however, reversible and can contribute to the enhancement of the specific capacitance in the form of “pseudocapacitance”. Phosphonium-based ILs are shown to possess a higher electrochemical stability, as compared to the ammonium-based ILs.³⁶ Indeed, [P_{6,6,6,14}][EHS] and [P_{4,4,4,4}][EHS] in this study are electrochemically stable even between -2.5 and +2.5 V, thus, their ECWs are at least 5 V at near-room temperatures.

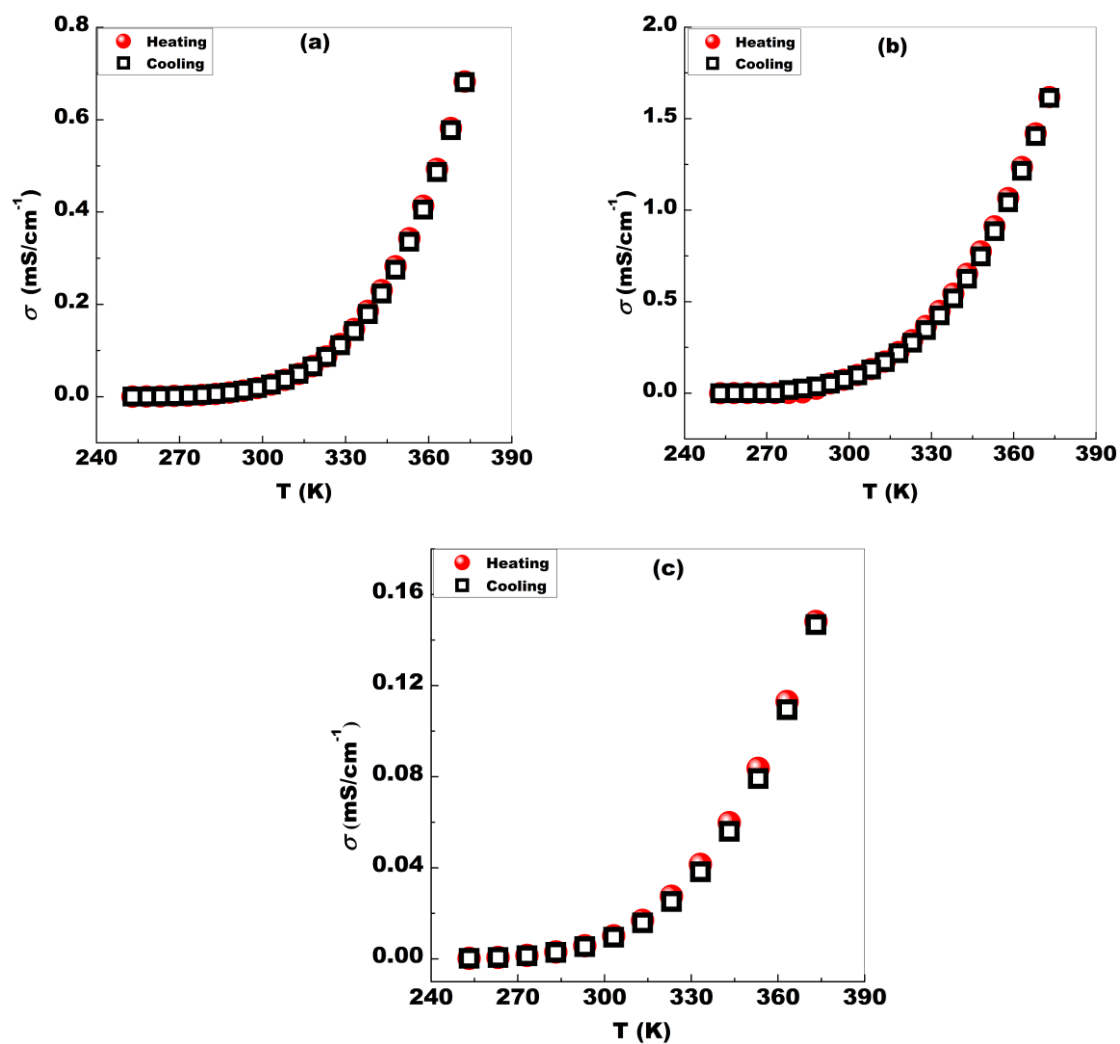


Figure 3. Comparative (heating – red circles, cooling – black open squares) electrical conductivity data of neat [P_{4,4,4,4}][EHS] (a), [C₆C₁Im][EHS] (b) and [P_{6,6,6,14}][EHS] (c), on GC electrodes at the AC voltage amplitude of 10 mV.

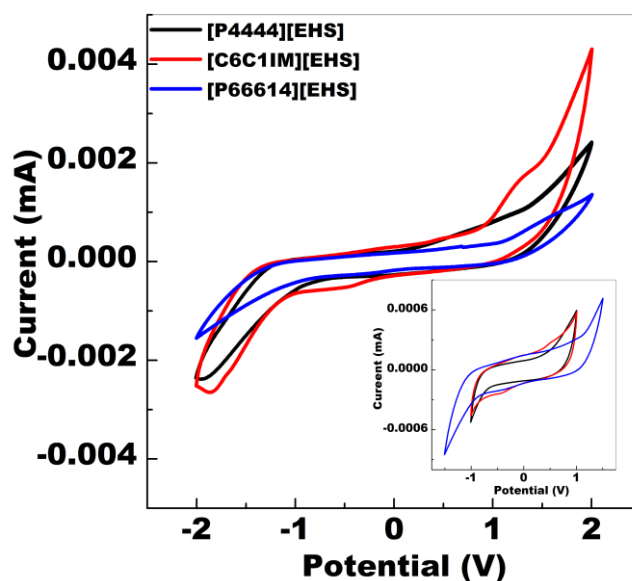


Figure 4. CV curves (from -2 to +2 V) for neat [C₆C₁Im][EHS] (red), [P_{4,4,4,4}][EHS] (black) and [P_{6,6,6,14}][EHS] (blue) on GC electrodes obtained at the scan rate of 100 mV s⁻¹ and at 298 K. Inset shows CV curves (from -1 to +1 V) for [P_{4,4,4,4}][EHS], [C₆C₁Im][EHS] and from -1.5 to +1.5 V for [P_{6,6,6,14}][EHS].

Thermal Characterisation of SAILs by DSC and TGA

The thermal stability of ILs mainly depends on the structure of constituent ions (cations and anions) and their interionic interactions. Thermal properties of the neat SAILs in this study were examined by the thermal gravimetric analysis (TGA) and differential scanning calorimetry (DSC). The TG plots and DSC traces of the studied SAILs are shown in **Figures 5** and **6**, respectively. The decomposition temperature (T_d), melting and crystallisation temperatures were measured by TGA and DSC, respectively. The T_d of a given IL depends on the inherent stability of the ionic liquid and interactions between their constituent ions. The TG plots show the decomposition pathway of [C₆C₁Im][EHS], [P_{4,4,4,4}][EHS] and [P_{6,6,6,14}][EHS] at 10 K min⁻¹ (see **Figure 5**) and degradation temperature values are also reported at different (2, 5 and 10) weight loss % in **Table S2**. This is in accordance with other studies, which revealed that imidazolium-based ionic liquids are thermally less stable than phosphonium-based ILs (with the same anions), but more thermally stable than the corresponding ammonium-based ionic liquids.³⁷ Differences in the thermal properties of SAILs studied here are mainly coming from the cationic part, as the same anion was used. A DSC trace of [C₆C₁Im][EHS] in **Figure 6** shows a couple of thermal events during heating and cooling scans.

During the heating cycle at 10 K min^{-1} from 213 K, two thermal events take place at 257 K (crystallisation) and 298 K (melting), while for the cooling cycle only one event was observed at 265 K, which corresponds to crystallisation of this SAIL. The other two SAILS in this study, show no distinct thermal events in the temperature range from 213 to 373 K (see **Figure 6**). Therefore, the latter two SAILS can be used as electrolytes in a wider range of temperatures, compared to $[\text{C}_6\text{C}_1\text{Im}][\text{EHS}]$. The heating and cooling ramp in DSC scans was chosen 10 K min^{-1} . All further heating and cooling cycles are reproducible and similar to the first heating and second cooling cycles that additionally confirms a high purity of SAILS used in this study.

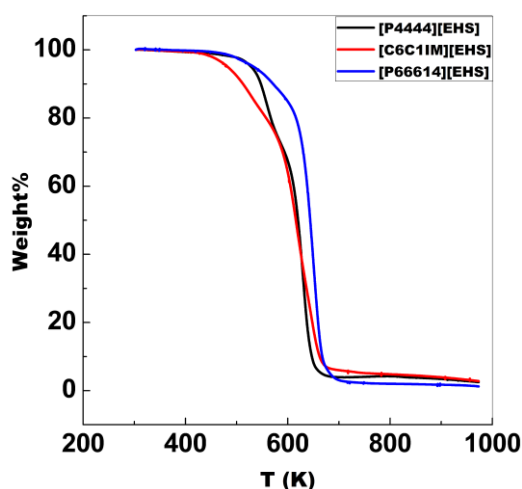


Figure 5. TG-plots of $[\text{C}_6\text{C}_1\text{Im}][\text{EHS}]$ (red), $[\text{P}_{4,4,4,4}][\text{EHS}]$ (black) and $[\text{P}_{6,6,6,14}][\text{EHS}]$ (blue) measured with the heating rate of 10 K min^{-1} in the temperature range from 303 to 973 K.

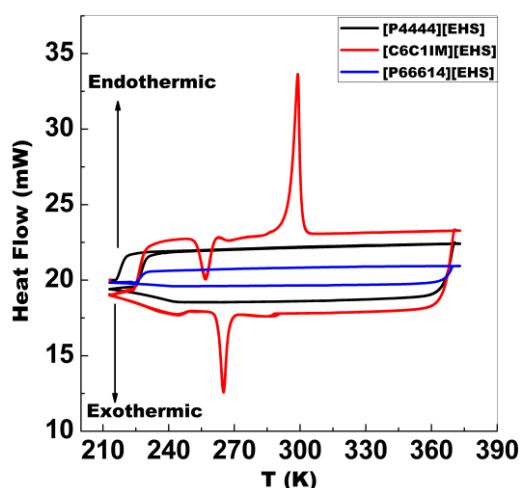


Figure 6. DSC traces for pure SAILS, $[\text{P}_{4,4,4,4}][\text{EHS}]$ (black), $[\text{C}_6\text{C}_1\text{Im}][\text{EHS}]$ (red), and $[\text{P}_{6,6,6,14}][\text{EHS}]$ (blue) at the heating rate of 10 K min^{-1} .

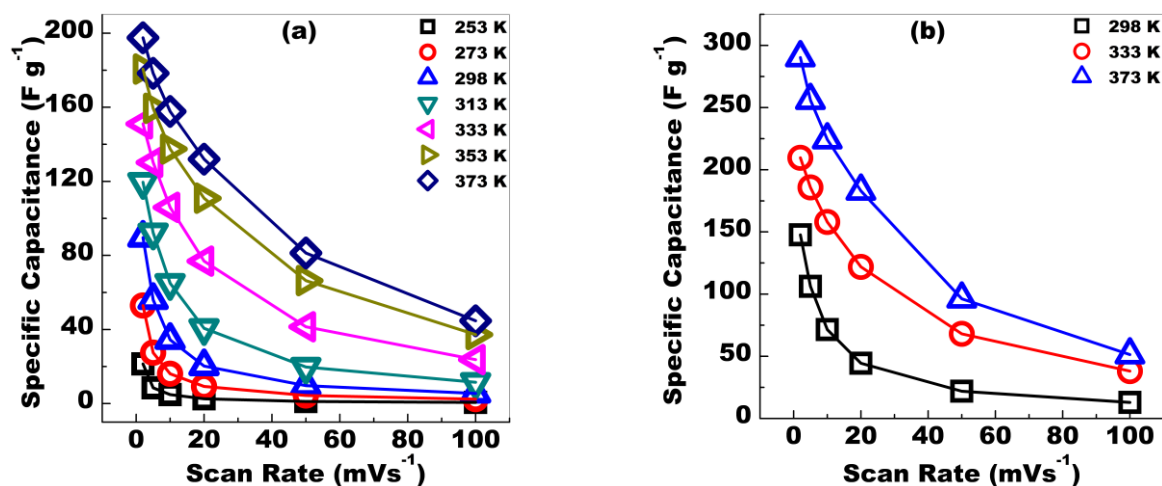
Therefore, a wide ECW, moderate ionic conductivity, a high thermal and electrochemical stability, and the presence of surface-active anions make these new SAILs as promising candidates for solvent-free electrolytes in high-energy storage devices such as supercapacitors, as will be explored further below.

Supercapacitor Measurements

Cyclic voltammetry (CV) curves were measured at different temperatures for the MWCNT-based electrode material and SAILs in this study, [P_{4,4,4,4}][EHS], [C₆C₁Im][EHS] and [P_{6,6,6,14}][EHS], as electrolytes (see **Figures S11, S12 and S13**, respectively, in the ESI). At 298, 313 and 333 K, CV curves measured at low scan rates (2, 5, 10 and 20 mV s⁻¹) have characteristic rectangular shapes. However, the shapes are more distorted at higher scan rates (at 50 and 100 mV s⁻¹). Interestingly, at even higher temperatures, 353 and 373 K, CV curves have rectangular shapes at all scan rates in this study that indicates a double-layer type of capacitance of the MWCNT-based supercapacitor with these SAILs. **Figure 7** shows variations of the specific capacitance (C_{elec}) with the electric potential scan rate for all the studied SAILs at different temperatures. Rectangular CV shapes indicate a good capacitive performance of the capacitor at lower scan rates at 298, 313 and 333 K. The capacitive performance is getting poorer at higher scan rates at these temperatures, but improved for all scan rates at 353 and 373 K. A poor capacitive performance at low temperatures may be ascribed to a low mobility of ions in electrolytes and a slow rearrangement of double layers of SAILs at surfaces of electrodes. In contrary, SAILs in this study show a better performance as electrolytes at high temperatures, when their viscosities decrease and ionic mobilities increase, without any chemical degradation and with a high electrochemical stability. A comparison between three SAILs in this study reveals that at the same experimental conditions of the scan rate, ECW of 4 V and temperature, [C₆C₁Im][EHS] shows higher specific capacitance values than those for [P_{4,4,4,4}][EHS] and [P_{6,6,6,14}][EHS] in the whole temperature range from 298 to 373 K.

The electric potential span for phosphonium-EHS SAILs can be increased from 4 to 5 V without any noticeable redox processes in a temperature range from 298 to 373 K: **Figure 7d** shows the specific capacitance values for a MWCNT/[P_{6,6,6,14}][EHS] capacitor and corresponding CV curves are shown in **Figure S14** in the ESI. When the ECW was increased from 4 to 5 V, a significant increase in the specific capacitance, by 35 - 80 %, was measured for the MWCNT/[P_{6,6,6,14}][EHS] system at ECW = 5 V (see **Figure 7d**) as compared to C_{elec} at ECW = 4 V (see **Figure 7c**). However, compared to the other two SAILs in this study,

[P_{6,6,6,14}][EHS] has much bulkier trihexyl(tetradecyl)phosphonium cations. Therefore, this SAIL is less appropriate for MWCNT-based electrodes, because charging/discharging and a double-layer capacitive behaviour depend on the pore size of the electrode material and the size of ions in electrolytes. Due to a significantly larger size of [P_{6,6,6,14}]⁺, these cations are less prone for adsorption into pores of MWCNTs with a diameter of less than 3-4 nm.³⁸ In this our study, SAILs were selected with the [EHS]⁻ anion of a smaller size as compared to that of anions in previously studied SAILs.¹⁶ A better performance of the MWCNT/SAILs capacitors was further achieved by the use of less bulky cations, such as [P_{4,4,4,4}]⁺ and [C₆C₁Im]⁺. Indeed, MWCNT/[C₆C₁Im][EHS] and MWCNT/[P_{4,4,4,4}][EHS] capacitors have two-three fold higher specific capacitance, energy density, and power density values in the whole range of temperatures in this study. Note that SAILs could be used in combination with other high surface area electrode materials to achieve even higher values for the specific capacitance and a better performance of supercapacitor devices (cyclic stability, electrochemical stability of electrolytes, etc.)³⁹⁻⁴²



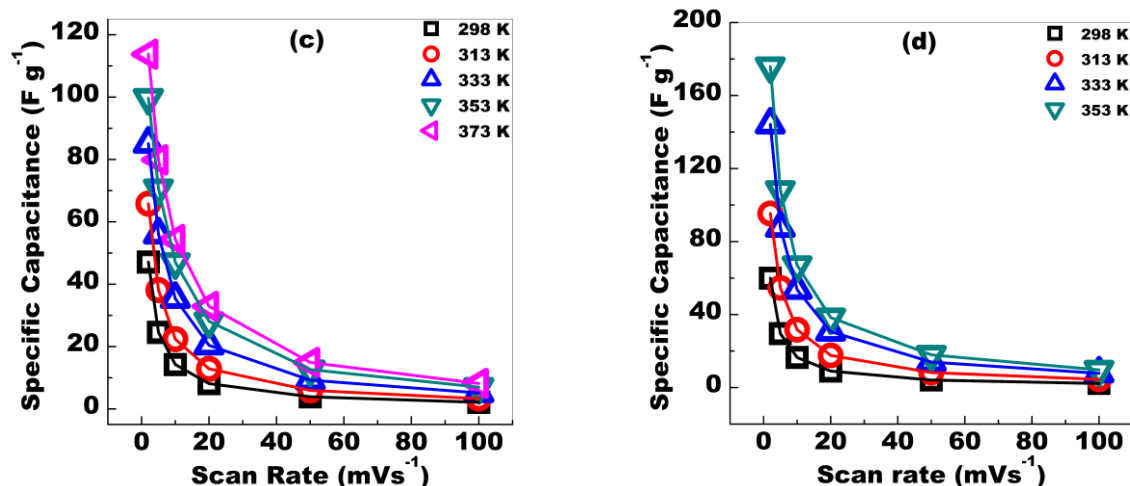


Figure 7. The specific capacitance values at different scan rates in the temperature range from 253 to 373 K at ECW of 4 V for [P_{4,4,4,4}][EHS] (a), [C₆C₁Im][EHS] (b) and [P_{6,6,6,14}][EHS] (c) and at ECW of 5 V for [P_{6,6,6,14}][EHS] (d).

The electrocapacitive performance of the SAILs also depends on their chemical structure as it might alter specific interactions between the SAIL and the electrode surface. A recent study provided an evidence that a SAIL may form stable electric double layers (EDLs) on electrode surfaces.¹⁶ A characteristic rectangular shape of CV curves at elevated temperatures and at high scan rates for MWCNTs/SAILs capacitors in this study is an indication of such stable EDL layers formed on MWCNTs that could be one of the reasons for a high specific capacitance of these devices, particularly for SAILs with less bulky cations, such as [C₆C₁Im]⁺ and [P_{4,4,4,4}]⁺. The specific capacitance values of supercapacitor MWCNTs/SAILs cells in this study range from 50 to 150 F g⁻¹ at 298 K, which are, actually, significantly higher than those reported in the literature for CNT-based capacitors with RTILs and other types of electrolytes (15-80 F g⁻¹ at ca. 298 K).⁴³⁻⁴⁶

It is interesting to compare shapes of CV curves for capacitors with MWCNTs electrodes and three different electrolytes in this study (see **Figures S11, S12 and S13** in the ESI) and their specific capacitance values as a function of scan rates and at different temperatures (see **Figure 7**). At low scan rates of 2 and 5 mV s⁻¹ and at T > 313 K, shapes of CV-curves are almost rectangular for all the studied SAILs. However, CV-curves become more and more distorted upon an increase in the scan rate, specifically at T < 333 K for capacitors with [P_{6,6,6,14}][EHS] and [P_{4,4,4,4}][EHS] as electrolytes (see **Figures S11 and S13** in the ESI) and these distortions are more pronounced at temperatures below 313 K. Interestingly, for [C₆C₁Im][EHS], the

“rectangular” shape of CV-curves remains almost undistorted up to scan rates of 50 and 100 mV s^{-1} at 333 and 373 K, (see **Figures S12b** and **S12c** in the ESI). Both shapes of CV curves and the specific capacitance values indicate that $[\text{C}_6\text{C}_1\text{Im}][\text{EHS}]$ does perform as a good electrolyte in MWCNTs-based supercapacitors in a wide temperature range from 298 to 373 K, but preferably at temperatures above 333 K. These facts are in a good agreement with previously reported data for SAILs with other types of bulky anions (1,4-bis(2-ethylhexoxy)-1,4-dioxobutane-2-sulfonate (AOT)).¹⁶ This our study suggests that more stable and more mobile EDLs are formed on MWCNTs electrodes for SAILs with less bulky cations ($[\text{C}_6\text{C}_1\text{Im}]^+$ and $[\text{P}_{4,4,4,4}]^+$), compared to SAILs with the same anion $[\text{EHS}]^-$, but more bulky cations, such as $[\text{P}_{6,6,6,14}]^+$ (this study) and $[\text{N}_{8,8,8,8}]^+$ ¹² even at high scan rates and at elevated temperatures ($T > 333$ K). For neat SAILs, an increase in temperature facilitates an increase in the mobility of ions, their approach to and reorientation at surfaces of electrodes and, hence, the ability of SAILs to form stable EDLs. The ionic conductivity (see **Figure 3**) and, thus, the mobility of ions in $[\text{C}_6\text{C}_1\text{Im}][\text{EHS}]$ is significantly higher as compared to those of $[\text{P}_{4,4,4,4}][\text{EHS}]$ and $[\text{P}_{6,6,6,14}][\text{EHS}]$ even at lower temperatures in this study, 298 and 313 K. Interactions between the constituent ions, which may lead to strong ion-pairing and a low ionicity in ILs, also control the ionic conductivity and the mobility of ions. Imidazolium-based ILs are known to have more mobile ions than tetraalkylammonium- and tetraalkylphosphonium-based ILs.⁴⁷ The latter can be explained by the fact that the positive (+1)-charge of the imidazolium cation is delocalised on nitrogen and carbon atoms of the imidazolium heterocycle, which results in a weaker coulombic interaction between ions and a higher ionicity in imidazolium-based ILs.^{47, 48} Therefore, more free ions are available in $[\text{C}_6\text{C}_1\text{Im}][\text{EHS}]$ as compared to $[\text{P}_{4,4,4,4}][\text{EHS}]$ and $[\text{P}_{6,6,6,14}][\text{EHS}]$ that results in higher specific capacitance values for MWCNTs/ $[\text{C}_6\text{C}_1\text{Im}][\text{EHS}]$ capacitors compared to those of the other two electrolytes in this study.

We further investigated the energy storage performance of the SAILs in this study. The ECW for aqueous electrolytes is only 1 V and that for other organic solvent-based electrolytes is around 1.5-3 V, while the ECW for the neat SAILs in this work is between 4 and 5 V in a temperature range from 298 to 373 K. Due to a wider ECW, the energy density of a capacitor is significantly larger for MWCNTs-based supercapacitors with neat SAILs as electrolytes when compared to aqueous- and organic-solvent-based electrolytes. The order of the specific capacitance and energy densities calculated from CV curves obtained at a scan rate of 2 mV s^{-1} is the following: $[\text{C}_6\text{C}_1\text{Im}][\text{EHS}] > [\text{P}_{4,4,4,4}][\text{EHS}] > [\text{N}_{8,8,8,8}][\text{EHS}] > [\text{P}_{6,6,6,14}][\text{EHS}]$ in the whole temperature range studied (see **Figures 8(a)** and **8(b)**). (**Figure S15** in the ESI shows

CV curves obtained at 2 mV s^{-1} for MWCNTs/[C₆C₁Im][EHS] and MWCNTs/[P_{4,4,4,4}][EHS] capacitors at different temperatures.) The data for tests on a MWCNTs/[N_{8,8,8,8}][EHS] capacitor was taken from our previous study.¹² The energy density and the power density values at different scan rates for MWCNTs/SAILs supercapacitors are also shown in **Figures S16** and **S17** in the ESI. Note that [P_{4,4,4,4}][EHS] can be used as an electrolyte even at rather low temperatures, 253 and 273 K, but both the specific capacitance and the energy density are very low at these temperatures, because of a low ionic mobility in the SAIL at these temperatures (see **Figures 8 (a)** and **8(b)**).

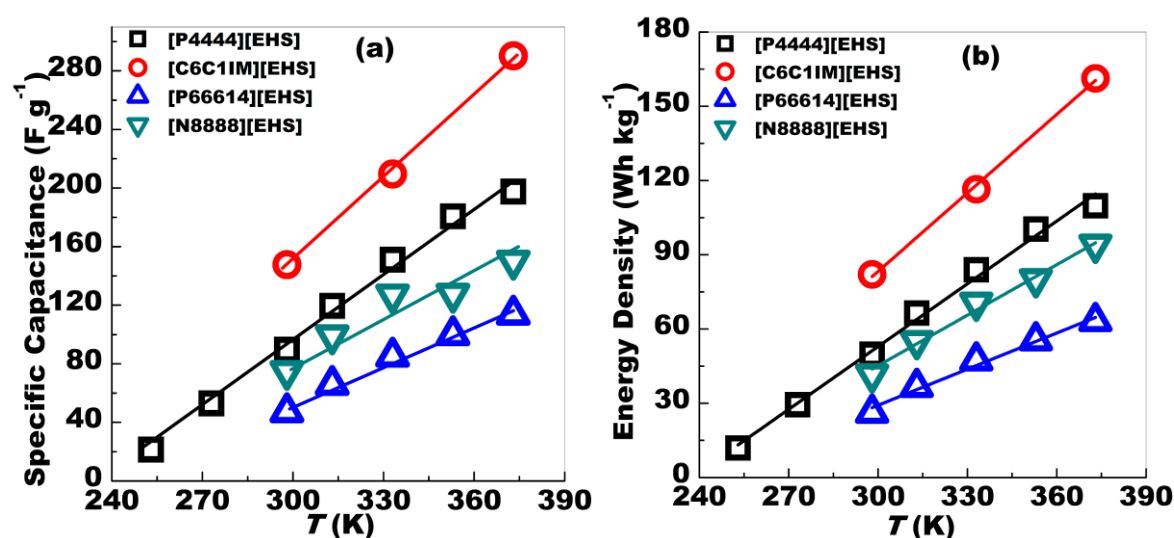


Figure 8. The specific capacitance (a), and the energy density (b) of MWCNTs/SAILs capacitors calculated from CV curves obtained at 2 mV s^{-1} and at different temperatures.

Supercapacitors with [P_{6,6,6,14}][EHS], [N_{8,8,8,8}][EHS] and [P_{4,4,4,4}][EHS] as electrolytes have rather low specific capacitance values, these SAILs can, in principle, be used in a wide temperature interval, from 253 to 373 K. In contrary, a WMCNTs-based supercapacitor with [C₆C₁Im][EHS] as an electrolyte has high specific capacitance values (from ca. 140 to 290 F g⁻¹ at 298 to 373 K, respectively) and these devices can be used at and above the room temperature, because this SAIL has its melting point at ca. 298 K. However, at higher temperatures both [P_{4,4,4,4}][EHS] and [C₆C₁Im][EHS] outperform the other two electrolytes ([P_{6,6,6,14}][EHS] and [N_{8,8,8,8}][EHS])¹² in terms of both the specific capacitance and the energy density. Therefore, both [C₆C₁Im][EHS] and [P_{4,4,4,4}][EHS] can be considered as suitable electrolytes for electric storage applications in a wide temperature range, at least from 298 to 373 K.⁴⁹ Many conventional aqueous (for example, 6 M KOH(aq)) and organic-solvent-based

electrolyte solutions have low boiling points and a low thermal stability that limit their use at high temperatures.^{25, 50, 51} For comparison, the specific capacitance, the energy density and the power density values of a MWCNTs/[P_{4,4,4,4}][EHS] are tabulated in **Table 1**. The data in this table was calculated from CV curves (see **Figure S18** in the ESI) obtained at scan rates of 2 and 5 mV s⁻¹, ECW of 5 V and at two different temperatures, 298 and 373 K, i.e. with four different sets of parameters. Note that different sets of the experimental parameters result in optimum values for the specific capacitance and the energy density (at 2 mV s⁻¹ and 373 K) and the power density (at 5 mV s⁻¹ and 373 K). Therefore, the performance of this type of supercapacitors can be further optimised depending on specific applications of this type of electric devices.

Table 1. The specific capacitance, the energy density and the power density of a MWCNTs/[P_{4,4,4,4}][EHS] supercapacitor at 298 and 373 K with ECW = 5 V.

Temperature (K)/ Scan Rate	2 mV s ⁻¹			5 mV s ⁻¹		
	C_{elec} (F g ⁻¹)	Energy Density (Wh kg ⁻¹)	Power density (kW kg ⁻¹)	C_{elec} (F g ⁻¹)	Energy Density (Wh kg ⁻¹)	Power density (kW kg ⁻¹)
298	132	74	106	87	48	174
373	285	158	228	229	127	458

Similarly, high values for the energy density and the power density were obtained at scan rates of 2 and 5 mV s⁻¹ for a MWCNTs/[P_{6,6,6,14}][EHS] capacitor at different temperatures in the electrochemical potential window of 5 V (from -2.5 to +2.5 V) (see **Figure S19** in the ESI). Therefore, both MWCNTs/[P_{4,4,4,4}][EHS] and MWCNTs/[P_{6,6,6,14}][EHS] can be used in high energy storage devices with ECW up to 5 V, particularly, at elevated temperatures, to facilitate high values for the specific capacitance, the energy density and the power density.

To further compare the effect of size and structure of cations, [C₆C₁Im]⁺, [P_{4,4,4,4}]⁺ and [P_{6,6,6,14}]⁺ on the performance of supercapacitors, we performed a range of additional electrochemical measurements on MWCNTs/SAILs devices.

Electrochemical Impedance Spectroscopy (EIS):

The EIS analysis provides a more fundamental understanding of electrode/electrolyte interface behaviour, ion diffusion and bulk properties of the electrolytes, etc., all important for a good

performance of electric energy storage devices.⁵²⁻⁵⁴ The EIS data analysis provides the charge-transfer resistance (R_{ct}) and the solution resistance (R_s) as a function of AC frequency. **Figure 9** shows the impedance spectra (Nyquist plots) of SAILs in this study at different temperatures. The Nyquist plots show a semicircle in the high frequency region, the Warburg line in the intermediate frequency region and almost a vertical line in the low frequency region, reflecting details of the charge storage mechanism of a system under study.⁵⁵ Nyquist plots were fitted using a modified Randal's circuit (see **Figure S20** in the ESI) with RelaxIS 3 software. The circuit in this analysis comprises R_s (solution resistance), R_{ct} (charge transfer resistance), CPE (constant phase element), W (Warburg component), and C_{dl} (double layer capacitance). The Warburg diffusion regions (with slopes $\sim 45^\circ$ from the horizontal axes) are clearly visible in Nyquist plots for SAILs in this study (see **Figure 9**). Steeper slopes signify higher diffusivity of ions entering the pores in electrodes, which is more prominent for [C₆C₁Im][EHS] compared to [P_{4,4,4,4}][EHS] and [P_{6,6,6,14}][EHS] (see insets in **Figure 9**). The steep rising trend of the imaginary part ($-Z''$) with respect to the real part (Z') of the impedance in the lower frequency range is observed in Nyquist plots for the SAILs particularly at high temperatures (333, 353 and 373 K) that shows a better capacitive behaviour of the capacitor. The intersection between the vertical line and the real Z' axis corresponds to the equivalent series resistance (ESR) and was estimated by an extrapolation method via Origin Pro 8.0 software. Values are given in **Table 3** (see also **Figure S21** in the ESI). The ESR shifted to lower values upon increasing the temperature, which confirms the increasing ion conductance and mobility at higher temperatures.

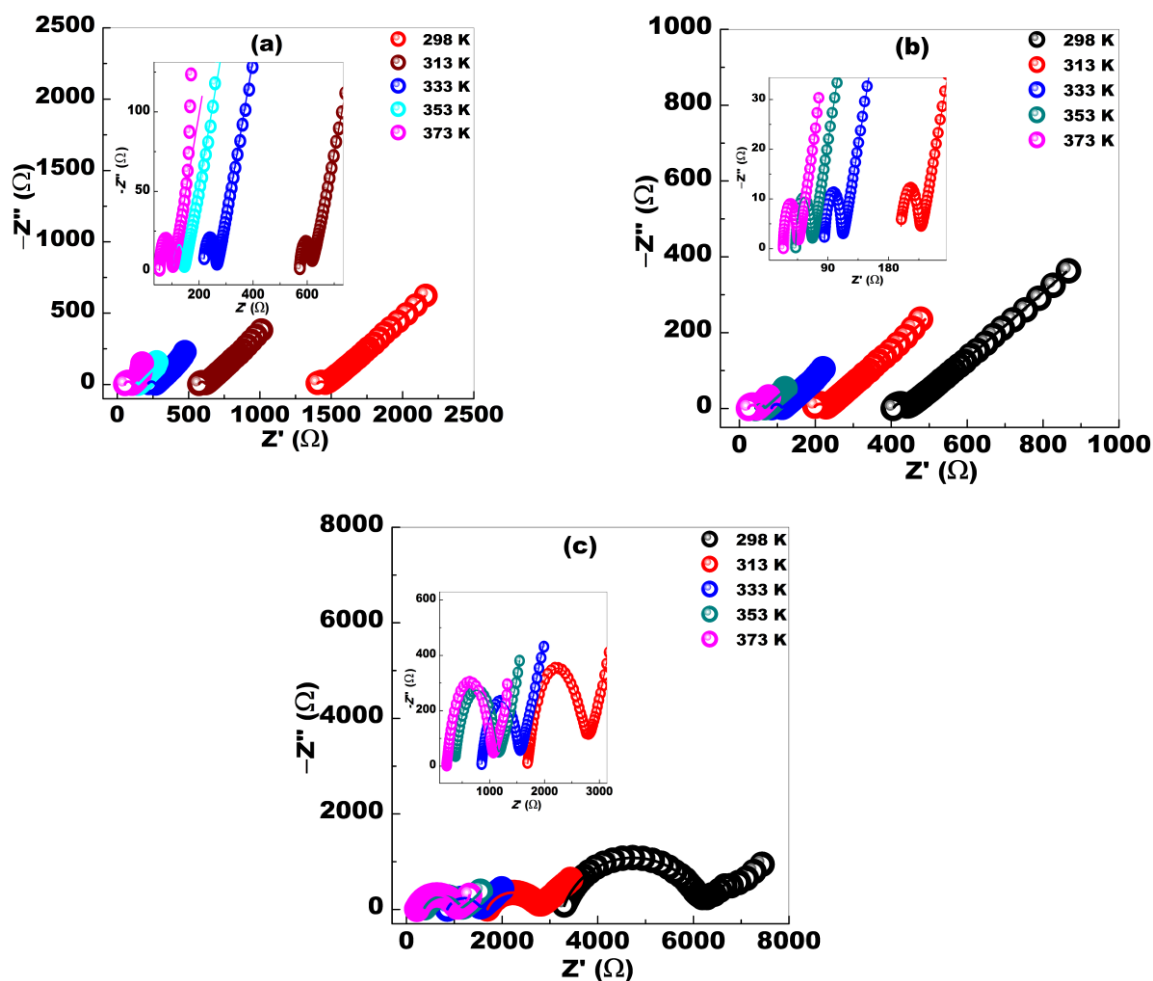


Figure 9. Nyquist plots at different temperatures for an MWCNT-based electrode with neat $[P_{4,4,4,4}][EHS]$ (a); $[C_6C_{1Im}][EHS]$ (b) and $[P_{6,6,6,14}][EHS]$ (c) as electrolytes.

The Nyquist plots show small semicircles in the high-frequency region for all SAILs in the order of $[C_6C_{1Im}][EHS] < [P_{4,4,4,4}][EHS] < [P_{6,6,6,14}][EHS]$ that confirms a faster charge transfer and a higher capacitance for $[C_6C_{1Im}][EHS]$ in the whole temperature range. The R_s and R_{ct} values are given in **Table 2** for a MWCNT-based electrode and different electrolytes. Also, for neat $[P_{4,4,4,4}][EHS]$, with an increase in temperature, the R_s and R_{ct} significantly decrease, from 1856 to 54 Ω and from 14510 to 48 Ω , respectively, for temperatures from 253 to 373 K. For $[P_{6,6,6,14}][EHS]$, corresponding values for both R_s and R_{ct} are much lower at the same temperatures.

Table 2. The solution resistance (R_s) and the charge transfer resistance (R_{ct}) values obtained from the Nyquist plots.

Temperature (K)	[C ₆ C ₁ Im][EHS]		[P _{4,4,4,4}][EHS]		[P _{6,6,6,14}][EHS]	
	R_s (Ω)	R_{ct} (Ω)	R_s (Ω)	R_{ct} (Ω)	R_s (Ω)	R_{ct} (Ω)
253			1856±130	14510±136		
273			1607±90	3631±15		
298	405±1	32±0.90	1398±1	136±3	3277±10	2890±18
313	196±1	28±0.68	570±1	37±1	1691±1	1080±2
333	84±0.15	26±0.40	215±1	52±1	853±1	691±1
353	42±0.08	23±0.20	105±1	42±1	686±1	878±2
373	24±0.19	21±0.32	54±1	48±1	217±1	846±2

Table 3. The equivalent series resistance (ESR) values obtained from the Nyquist plots by extrapolation.

Temperature (K)	[C ₆ C ₁ Im][EHS]	[P _{4,4,4,4}][EHS]	[P _{6,6,6,14}][EHS]
333	221±2	468±5	1994±20
353	117±1	264±3	1517±15
373	72±1	163±1	1287±13

Galvanostatic Charge Discharge (GCD)

We further performed GCD experiments to check the performance of the capacitor. **Figure 10** shows comparative GCD curves for the SAILs/MWCNT-based supercapacitor at different temperatures. We observed that all curves have similar isosceles triangular shapes that represent a typical pattern of a satisfactory capacitor behaviour for the studied supercapacitors. A steep profile for IR_{drop} was observed for the SAILs at lower temperatures, 298 and 313 K at 0.14 A g⁻¹. Upon an increase in the current density, IR_{drop} further increased at these temperatures. This might be a result of a high viscosity of SAILs and a small pore size of the electrode material compared to the size of ions of the electrolyte. The IR_{drop} parameter corresponds to the ESR of the supercapacitor cell, which is associated with the diffusion mobility of the electrolyte ions travelling through the pores of the electrode. However, it can also be observed that the areas under the curve and the discharge period are different for each system in this study, being at a maximum at 373 K for the SAILs and exhibiting a better capacitive performance at 373 K compared to lower temperatures. The GCD curves at different current densities are provided in the ESI for [P_{4,4,4,4}][EHS] at 0.07 and 0.11 A g⁻¹ (see **Figure**

S22 in the ESI) and for [C₆C₁Im][EHS] at 0.11 A g⁻¹ (see **Figure S23** in the ESI). Whereas, for [P_{6,6,6,14}][EHS] GCD curves were obtained only at a very low current density of 0.014 A g⁻¹ (see **Figure S24** in the ESI) due to a high viscosity of this SAIL. The specific capacitance values were calculated from the GCD curves using the following equation:⁵⁶

$$C_{elec} = 4 \frac{I\Delta t}{m\Delta V} \quad (4)$$

where, Δt is the discharge time, ΔV is the voltage difference, I is current, and m is a mass of the electrode.

Table 4 and **5** show values of C_{elec} (F g⁻¹) and the energy density, E (W h kg⁻¹) calculated from the GCD curves and CV curves at 10 mV s⁻¹ for [C₆C₁Im][EHS] and [P_{4,4,4,4}][EHS], respectively. The C_{elec} values obtained from GCD curves at lower current densities are in a good agreement with those obtained from the CV curves.

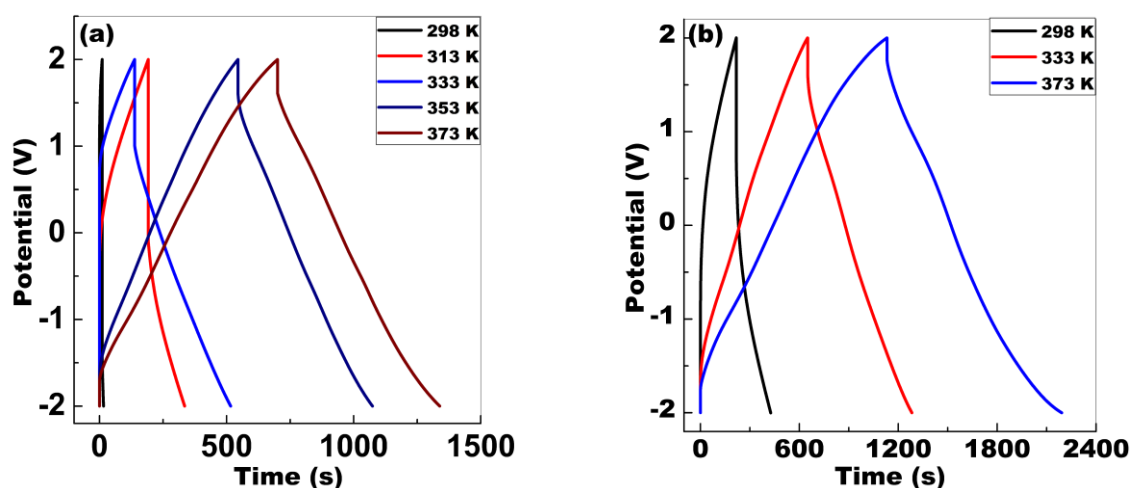


Figure 10. Galvanostatic charge discharge curves for an MWCNT-based electrode with neat [P_{4,4,4,4}][EHS] (a), and [C₆C₁Im][EHS] (b) as electrolytes, at 0.14 A g⁻¹ current density at different temperatures.

Table 4. Specific capacitance (C_{elec}) and the energy density (E) for a MWCNTs/[C₆C₁Im][EHS] capacitor.

Temperature (K)	CV at 10 mVs ⁻¹		GCD at 0.11 A g ⁻¹		GCD at 0.14 A g ⁻¹	
	C_{elec} (F g ⁻¹)	E (W h kg ⁻¹)	C_{elec} (F g ⁻¹)	E (W h kg ⁻¹)	C_{elec} (F g ⁻¹)	E (W h kg ⁻¹)
298	71	40	66	33	44	22
333	158	88	113	106	100	91
373	224	125	180	180	160	159

Table 5. Specific capacitance (C_{elec}) and the energy density (E) for a MWCNTs/[P_{4,4,4,4}][EHS] supercapacitor.

Temperature (K)	CV at 10 mV s ⁻¹		GCD at 0.07 A g ⁻¹		GCD at 0.11 A g ⁻¹		GCD at 0.14 A g ⁻¹	
	C_{elec} (F g ⁻¹)	E (W h kg ⁻¹)	C_{elec} (F g ⁻¹)	E (W h kg ⁻¹)	C_{elec} (F g ⁻¹)	E (W h kg ⁻¹)	C_{elec} (F g ⁻¹)	E (W h kg ⁻¹)
298	34	19	25	9	10	1	5	1
313	65	36	55	40	47	22	43	11
333	106	59	77	71	74	55	72	45
353	137	76	92	92	93	88	84	76
373	158	88	117	118	112	112	101	92

At the end of all aforementioned experiments, 500 CV cycles with a scan rate of 50 mV s⁻¹ at 298 and 333 K were recorded for an MWCNT-based electrode with [C₆C₁Im][EHS] and [P_{4,4,4,4}][EHS] as electrolytes, respectively. For [P_{6,6,6,14}][EHS], 100 cycles were recorded at 25 mV s⁻¹ at 298 K and 50 cycles were recorded at 25 mV s⁻¹ at 373 K. **Figure 11** shows that [P_{4,4,4,4}][EHS] exhibited a good capacitance retention (98%), for [C₆C₁Im][EHS] the capacitance increased with the number of cycles. For [P_{6,6,6,14}][EHS], 99% retention was observed in capacitance after completing all the experiments. **Figures S25** and **S26** in the ESI show a well-overlapping CV-curves (the first and the last CV cycles). The EIS measurements were also performed before and after cyclic tests and showed a good overlap of the EIS data (see **Figure S27** in the ESI). After completion of all the experiments from 298 to 373 K and the cyclic tests, the CV show good overlaps (see **Figure S28** in the ESI) for the studied SAILs, which indicates a good thermal and electrochemical stability of all SAILs in this study.

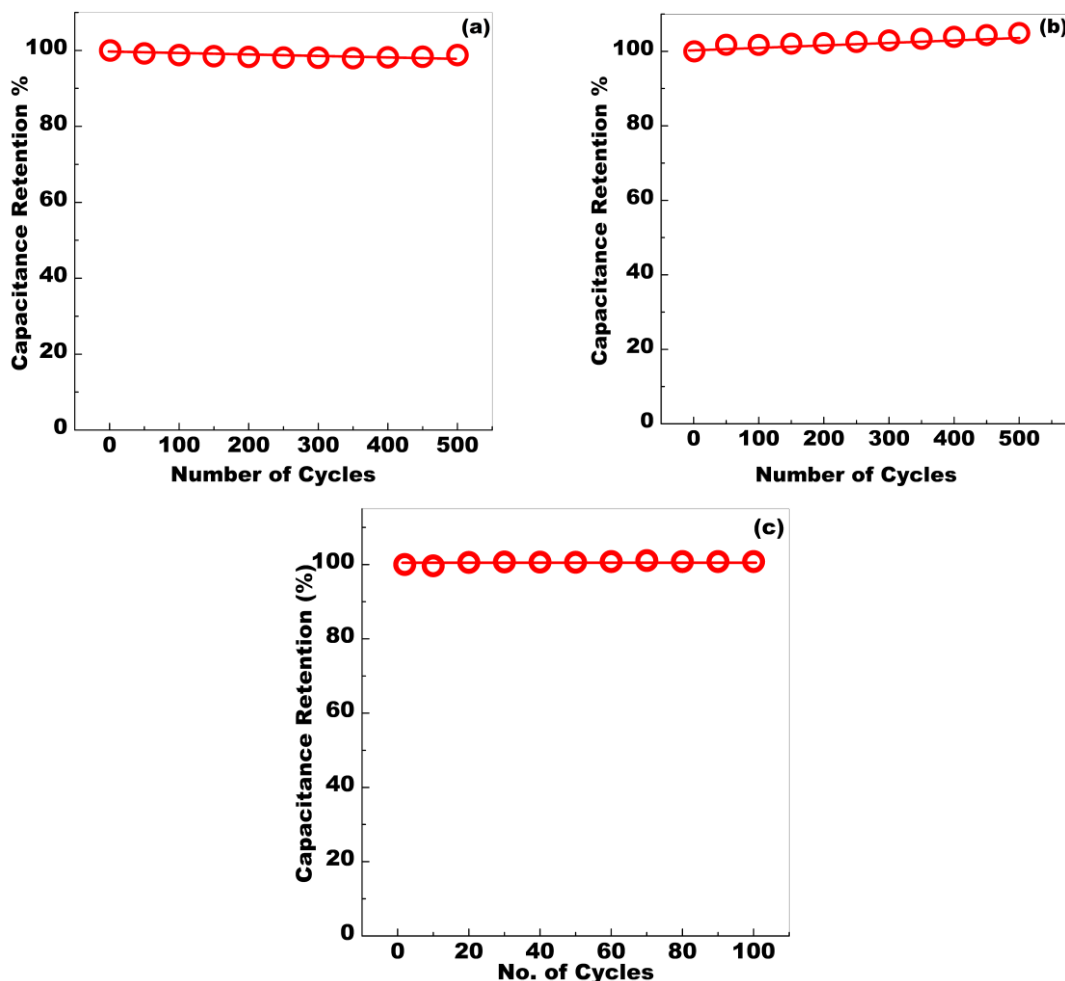


Figure 11. Capacitance retention of CV cycles at the scan rate of 50 mV s^{-1} and at 333 K after completing all the experiments up to 373 K for a MWCNTs/[P_{4,4,4,4}][EHS] supercapacitor (a); at 50 mV s^{-1} and 298 K for a MWCNTs/[C₆C₁Im][EHS] supercapacitor (b) and at 25 mV s^{-1} and 298 K for a MWCNTs/[P_{6,6,6,14}][EHS] supercapacitor (c).

Ragone plot

We further quantified the power density and the energy density of the MWCNTs/SAILs supercapacitors in this study, as it is a crucial parameter in choosing an appropriate electrode-electrolyte combination. The power density, P , and the energy density, E , calculated using Eqs. (2) and (3) were plotted against each other and generally referred as the Ragone plot. **Figure 12** shows that MWCNTs/[C₆C₁Im][EHS] outperforms other supercapacitors in this study in the temperature range from 298 to 373 K. A comparison between the Ragone plots for all SAILs in this study at different temperatures infers that [C₆C₁Im][EHS] has higher values for both the energy density and the power densities as compared to the other two SAIL electrolytes.

For a MWCNTs/[C₆C₁Im][EHS] supercapacitor at the scan rate of 2 mV s⁻¹ and at 298 K, the energy density and the power density values were 82 W h kg⁻¹ and 148 kW kg⁻¹, respectively. These values can further be improved upon increasing the temperature to 373 K, but keeping the scan rate the same (2 mV s⁻¹): both the energy density (161 W h kg⁻¹) and the power density (290 kW kg⁻¹) were almost doubled. Upon an increase of temperature from 298 to 373 K, both the energy density and the power density have also increased for MWCNTs/[P_{4,4,4,4}][EHS] and MWCNTs/[P_{6,6,6,14}][EHS] supercapacitors: from 50 to 110 W h kg⁻¹ and 90 to 198 kW kg⁻¹; and 26 to 63 W h kg⁻¹ and 47 to 114 kW kg⁻¹, respectively. The electrochemical performance of studied supercapacitors is significantly better than that reported for MWCNTs/halogenated ILs as electrolytes.⁵⁷⁻⁶⁰

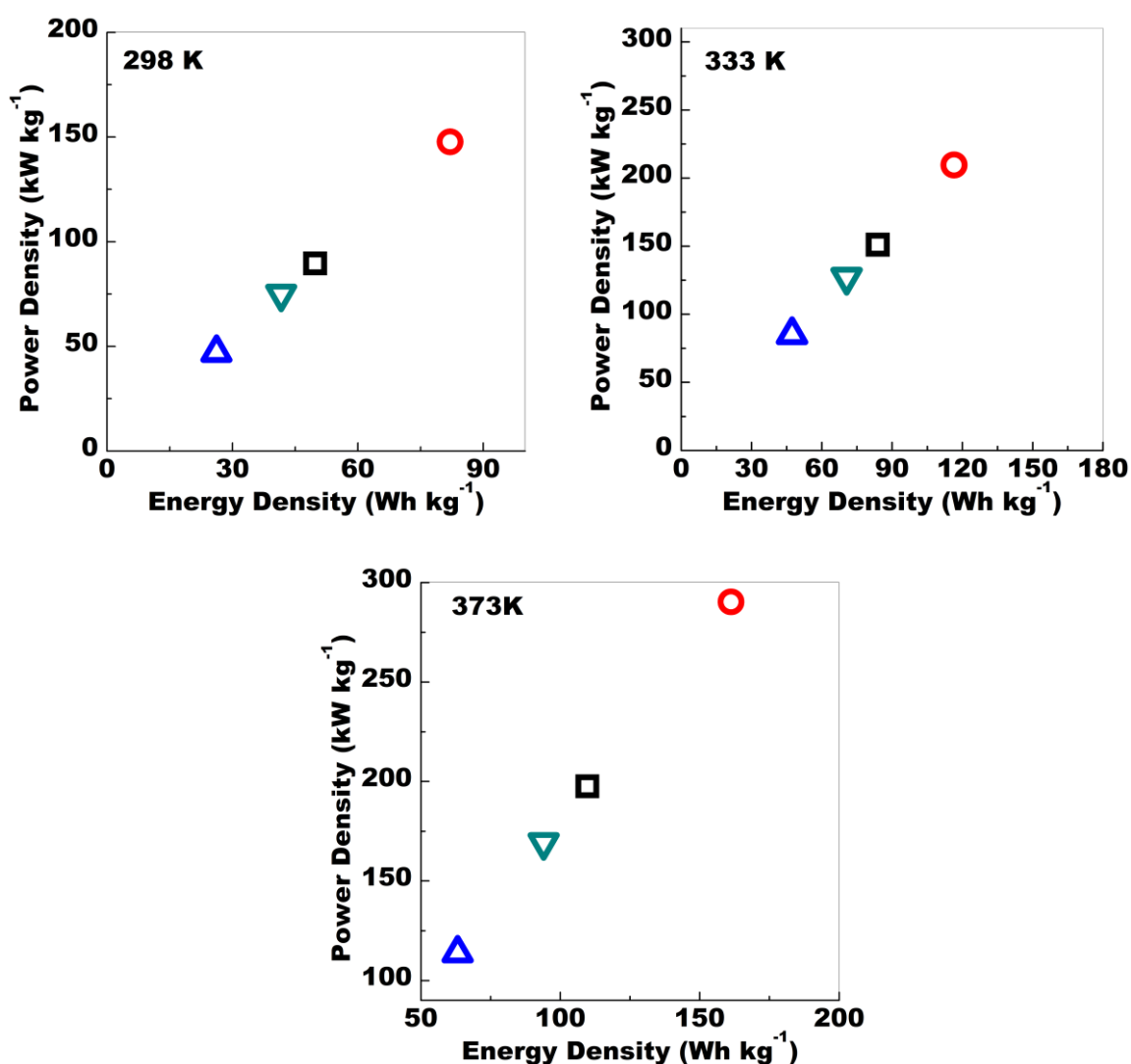


Figure 12. Ragone plots for MWCNT/SAILs capacitors with SAILs as following: [C₆C₁Im][EHS] (○), [P_{4,4,4,4}][EHS] (□), [P_{6,6,6,14}][EHS] (△), and [N_{8,8,8,8}][EHS] (▽)¹². Data obtained at the scan rate of 2 mV s⁻¹ at different temperatures, 298, 333 and 373 K.

After a thorough comparative analysis, we conclude that SAILs, such as [C₆C₁Im][EHS], [P_{4,4,4,4}][EHS], [P_{6,6,6,14}][EHS] from this study and [N_{8,8,8,8}][EHS] (from our previous study)¹² can be considered a value-added electrolytes in MWCNTs-based supercapacitor devices with a high specific capacitance, energy density and power density over a wide operating temperature range and with a good thermal, chemical and electrochemical stability. Comparing supercapacitors with different electrode materials and electrolytes, mainly ionic liquids, reported previously, we infer that the MWCNTs-based supercapacitors in combination with SAILs from the current study perform satisfactorily well in a wide range of temperatures. Data for aqueous, organic and IL-based electrolytes are also given for comparison in the Ragone plot in **Figure 13**. The latter plot shows that studied here SAILs outperform other up-to-now reported electrolytes in terms of combined the power density and the energy density performance.

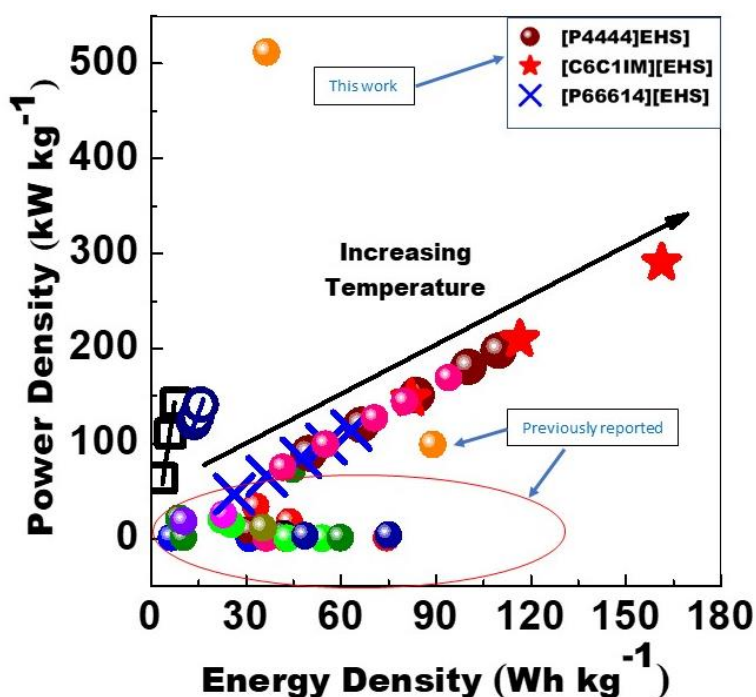


Figure 13. Ragone plots for a supercapacitor cell with MWCNT-based electrodes and neat [P_{4,4,4,4}][EHS] (brown solid circles), [C₆C₁Im][EHS] (red solid star), and [P_{6,6,6,14}][EHS] (blue cross). (*P* and *E* were calculated from CV curves obtained at a scan rate of 2 mV s⁻¹). 6 M

KOH(aq) (black squares), neat [N_{8,8,8,8}][EHS] (pink solid circles), 50:50 wt% binary mixture of [N_{8,8,8,8}][EHS] with AcN as electrolytes (dark-blue open circles) from ref.¹² All other solid data points have been taken from the literature for a comparison; blue⁵⁷, wine⁵⁸, royal blue⁶⁰, red⁶¹, black⁶², pink⁶³, green⁶⁴, olive⁶⁵, orange⁶⁶, violet⁶⁷, dark yellow⁶⁸ and magenta⁶⁹.

Conclusions

Novel room-temperature surface active ionic liquids (SAILs) composed of different cations ([P_{4,4,4,4}]⁺, [C₆C₁Im]⁺, ([P_{6,6,6,14}]⁺) and the 2-ethylhexyl sulfate anion ([EHS]⁻) were synthesised and thoroughly characterised as electrolytes in MWCNTs-based supercapacitors. Interestingly, these non-halogenated SAILs with the [EHS]⁻ as anion are liquids in a wide temperature range, whereas other halogenated ILs containing tetrabutylphosphonium or tetraalkylammonium as cations and halogen-containing anions, are solid in nature. The specific capacitance values (C_{elec}) for MWCNTs/SAILs systems in this study are comparable or even higher to those previously reported for other types of SAILs. This study further validates a recently suggested concept that SAILs can be used as improved and safer electrolytes in supercapacitor cells in a wide range of temperatures and at extended electrochemical potential windows (ECW) to 4-5 V that is much wider than ECWs of aqueous and organic solvent-based electrolytes. The studied SAILs are economical and environmentally benign. Therefore, they can be used at a large scale without polluting the environment. The degradation temperature of SAILs in this study is above 550 K. Therefore, MWCNTs/SAILs systems could potentially be further studied even above 373 K, which is the temperature limit of Autolab potentiostat used in this study. At 298 K and at the scan rate of 2 mV s⁻¹ and ECW = 4 V, the specific capacitance was measured to be 148, 90 and 47 F g⁻¹ for supercapacitors with MWCNT-based electrodes and [C₆C₁Im][EHS], [P_{4,4,4,4}][EHS] and [P_{6,6,6,14}][EHS] as electrolytes, while the energy density values were 82, 50, and 26 W h kg⁻¹, respectively. From a three- to four-fold increase in the specific capacitance and the energy density values was measured for the afore above systems at the same experimental conditions, but upon an increase of temperature to 373 K: 290, 198 and 114 F g⁻¹ and 161, 110 and 63 W h kg⁻¹, respectively. Therefore, these novel SAILs can be considered as suitable electrolytes for high-temperature applications, such as powering energy devices in the oil and gas industries and in military and space applications. Overall, MWCNTs/[C₆C₁Im][EHS] and MWCNTs/[P_{4,4,4,4}][EHS] supercapacitors outperformed other systems with SAILs electrolytes in this and previous studies at variable temperatures and in a

wide electrochemical potential range (4-5 V) along with a good thermal, electrochemical and cyclic stability of these SAILs. Therefore, both [C₆C₁Im][EHS] and [P_{4,4,4,4}][EHS] can be considered as “electrolytes-of-the-choice” in various high-temperature applications. This paves the way for building “designer” SAILs, since there is a large number of possible anion-cation combinations, which can be exploited to develop non-halogenated and environmentally benign ILs for next-generation electric energy storage devices.

Conflicts of Interest

There are no conflicts of interest to declare.

Acknowledgements

The Kempe Foundation in memory of J. C. and Seth M. Kempe is gratefully acknowledged for the financial support in the form of a stipend for P.J. (Grant No. JCK-1810), and for projects SMK-1945, JCK-1306 and JCK-1433 and the laboratory fund at LTU for providing grants, from which electrochemical equipment and a 400 MHz Bruker Aeon/Avance III NMR spectrometer at LTU have been purchased.

References:

1. Z. Lei, B. Chen, Y. M. Koo and D. R. MacFarlane, *Chem. Rev.*, 2017, **117**, 6633-6635.
2. M. Galiński, A. Lewandowski and I. Stępniaik, *Electrochim. Acta*, 2006, **51**, 5567-5580.
3. M. J. Earle and K. R. Seddon, *Clean Solvents*, 2002, **819**, 10-25.
4. M. Armand, F. Endres, D. R. MacFarlane, H. Ohno and B. Scrosati, *Nat. Mater.*, 2009, **8**, 621-629.
5. D. R. MacFarlane, M. Forsyth, P. C. Howlett, M. Kar, S. Passerini, J. M. Pringle, H. Ohno, M. Watanabe, F. Yan, W. J. Zheng, S. G. Zhang and J. Zhang, *Nat. Rev. Mater.*, 2016, **1**, 15005, 1-15.
6. A. Brandt, S. Pohlmann, A. Varzi, A. Balducci and S. Passerini, *MRS Bull.*, 2013, **38**, 554-559.
7. J. Z. Sun, D. R. MacFarlane and M. Forsyth, *Ionics*, 1997, **3**, 356-362.
8. J. Sun, M. Forsyth and D. R. MacFarlane, *J. Phys. Chem. B*, 1998, **102**, 8858-8864.
9. K. Tsunashima and M. Sugiya, *Electrochem. Commun.*, 2007, **9**, 2353-2358.
10. K. Shimizu, A. A. Padua and J. N. Canongia Lopes, *J. Phys. Chem. B*, 2010, **114**, 15635-15641.

11. P. J. Griffin, A. P. Holt, Y. Wang, V. N. Novikov, J. R. Sangoro, F. Kremer and A. P. Sokolov, *J. Phys. Chem. B*, 2014, **118**, 783-790.
12. P. Jain and O. N. Antzutkin, *ACS Appl. Energy Mater.*, 2021, DOI: 10.1021/acsaem.1c01157.
13. M. Hilder, G. M. A. Girard, K. Whitbread, S. Zavorine, M. Moser, D. Nucciarone, M. Forsyth, D. R. MacFarlane and P. C. Howlett, *Electrochim. Acta*, 2016, **202**, 100-109.
14. R. K. Blundell and P. Licence, *Phys. Chem. Chem. Phys.*, 2014, **16**, 15278-15288.
15. K. Yoshii, K. Yamaji, T. Tsuda, K. Tsunashima, H. Yoshida, M. Ozaki and S. Kuwabata, *J. Phys. Chem. B*, 2013, **117**, 15051-15059.
16. X. Mao, P. Brown, C. Cervinka, G. Hazell, H. Li, Y. Ren, D. Chen, R. Atkin, J. Eastoe, I. Grillo, A. A. H. Padua, M. F. Costa Gomes and T. A. Hatton, *Nat. Mater.*, 2019, **18**, 1350-1357.
17. S. Pan, M. Yao, J. Zhang, B. Li, C. Xing, X. Song, P. Su and H. Zhang, *Front Chem*, 2020, **8**, 261, 1-18.
18. T. M. Bandhauer, S. Garimella and T. F. Fuller, *J. Electrochem. Soc.*, 2011, **158**, R1-R25.
19. M. V. Fedorov and A. A. Kornyshev, *Chem. Rev.*, 2014, **114**, 2978-3036.
20. M. Salanne, B. Rotenberg, K. Naoi, K. Kaneko, P. L. Taberna, C. P. Grey, B. Dunn and P. Simon, *Nat. Energy*, 2016, **1**, 16070, 1-10.
21. M. Z. Bazant, B. D. Storey and A. A. Kornyshev, *Phys. Rev. Lett.*, 2012, **109**, 046102, 1-4.
22. M. A. Gebbie, H. A. Dobbs, M. Valtiner and J. N. Israelachvili, *Proc. Natl. Acad. Sci. USA*, 2015, **112**, 7432-7437.
23. H. Zhou, M. Rouha, G. Feng, S. S. Lee, H. Docherty, P. Fenter, P. T. Cummings, P. F. Fulvio, S. Dai, J. McDonough, V. Presser and Y. Gogotsi, *ACS Nano*, 2012, **6**, 9818-9827.
24. M. A. Gebbie, M. Valtiner, X. Banquy, E. T. Fox, W. A. Henderson and J. N. Israelachvili, *Proc. Natl. Acad. Sci. USA*, 2013, **110**, 9674-9679.
25. C. Zhong, Y. Deng, W. Hu, J. Qiao, L. Zhang and J. Zhang, *Chem. Soc. Rev.*, 2015, **44**, 7484-7539.
26. S. McDonald, T. Murphy, S. Imberti, G. G. Warr and R. Atkin, *J. Phys. Chem. Lett.*, 2018, **9**, 3922-3927.
27. P. Brown, C. P. Butts, J. Eastoe, D. Fermin, I. Grillo, H. C. Lee, D. Parker, D. Plana and R. M. Richardson, *Langmuir*, 2012, **28**, 2502-2509.

28. T. Y. Wu, S. G. Su, S. T. Gung, M. W. Lin, Y. C. Lin, C. A. Lai and I. W. Sun, *Electrochim. Acta*, 2010, **55**, 4475-4482.
29. J. D. Holbrey, W. M. Reichert, R. P. Swatloski, G. A. Broker, W. R. Pitner, K. R. Seddon and R. D. Rogers, *Green Chem.*, 2002, **4**, 407-413.
30. R. P. Swatloski, J. D. Holbrey and R. D. Rogers, *Green Chem.*, 2003, **5**, 361-363.
31. S. C. Canobre, D. A. L. Almeida, C. P. Fonseca and S. Neves, *Electrochim. Acta*, 2009, **54**, 6383-6388.
32. V. Khomenko, E. Raymundo-Piñero and F. Béguin, *J. Power Sources*, 2006, **153**, 183-190.
33. M. S. Wu and K. H. Lin, *J. Phys. Chem. C*, 2010, **114**, 6190-6196.
34. A. T. Chidembo, K. I. Ozoemena, B. O. Agboola, V. Gupta, G. G. Wildgoose and R. G. Compton, *Energy Environ. Sci.*, 2010, **3**, 228-236.
35. P. Jain, V. R. Chaudhari and A. Kumar, *Phys. Chem. Chem. Phys.*, 2019, **21**, 24126-24131.
36. A. I. Bhatt, I. May, V. A. Volkovich, M. E. Hetherington, B. Lewin, R. C. Thied and N. Ertok, *J. Chem. Soc., Dalton Trans.*, 2002, **24**, 4532-4534.
37. Y. Y. Cao and T. C. Mu, *Ind. Eng. Chem. Res.*, 2014, **53**, 8651-8664.
38. P. Simon and Y. Gogotsi, *Acc. Chem. Res.*, 2013, **46**, 1094-1103.
39. D. Pech, M. Brunet, H. Durou, P. Huang, V. Mochalin, Y. Gogotsi, P. L. Taberna and P. Simon, *Nat. Nanotechnol.*, 2010, **5**, 651-654.
40. K. Xie, X. Qin, X. Wang, Y. Wang, H. Tao, Q. Wu, L. Yang and Z. Hu, *Adv. Mater.*, 2012, **24**, 347-352.
41. X. W. Mao, X. Q. Yang, J. Wu, W. D. Tian, G. C. Rutledge and T. A. Hatton, *Chem. Mater.*, 2015, **27**, 4574-4585.
42. X. Mao, F. Simeon, G. C. Rutledge and T. A. Hatton, *Adv. Mater.*, 2013, **25**, 1309-1314.
43. S. H. Aboutalebi, A. T. Chidembo, M. Salari, K. Konstantinov, D. Wexler, H. K. Liu and S. X. Dou, *Energy Environ. Sci.*, 2011, **4**, 1855-1865.
44. E. Frackowiak, K. Jurewicz, S. Delpoux and F. Béguin, *J. Power Sources*, 2001, **97-8**, 822-825.
45. E. Frackowiak, K. Jurewicz, K. Szostak, S. Delpoux and F. Béguin, *Fuel Process. Technol.*, 2002, **77**, 213-219.
46. E. Frackowiak, S. Delpoux, K. Jurewicz, K. Szostak, D. Cazorla-Amoros and F. Béguin, *Chem. Phys. Lett.*, 2002, **361**, 35-41.

47. W. L. Yuan, X. Yang, L. He, Y. Xue, S. Qin and G. H. Tao, *Front. Chem.*, 2018, **6**, 59, 1-12.
48. T. Welton, *Biophys. Rev.*, 2018, **10**, 691-706.
49. X. Lin, M. Salari, L. M. Arava, P. M. Ajayan and M. W. Grinstaff, *Chem. Soc. Rev.*, 2016, **45**, 5848-5887.
50. R. S. Borges, A. L. Reddy, M. T. Rodrigues, H. Gullapalli, K. Balakrishnan, G. G. Silva and P. M. Ajayan, *Sci. Rep.*, 2013, **3**, 2572, 1-6.
51. P. Simon and Y. Gogotsi, *Nat. Mater.*, 2008, **7**, 845-854.
52. B. A. Mei, O. Munteshari, J. Lau, B. Dunn and L. Pilon, *J. Phys. Chem. C*, 2018, **122**, 194-206.
53. P. L. Taberna, P. Simon and J. F. Fauvarque, *J. Electrochem. Soc.*, 2003, **150**, A292-A300.
54. B. E. Conway, in *Electrochemical Supercapacitors: Scientific Fundamentals and Technological Applications*, ed. B. E. Conway, Springer US, Boston, MA, 1999, DOI: 10.1007/978-1-4757-3058-6_1, pp. 1-9.
55. Y. Xu, Z. Lin, X. Zhong, X. Huang, N. O. Weiss, Y. Huang and X. Duan, *Nat. Commun.*, 2014, **5**, 4554, 1-8.
56. M. D. Stoller and R. S. Ruoff, *Energy Environ. Sci.*, 2010, **3**, 1294-1301.
57. H. T. Liu and G. Y. Zhu, *J. Power Sources*, 2007, **171**, 1054-1061.
58. A. Balducci, R. Dugas, P. L. Taberna, P. Simon, D. Plée, M. Mastragostino and S. Passerini, *J. Power Sources*, 2007, **165**, 922-927.
59. R. S. Borges, H. Ribeiro, R. L. Lavall and G. G. Silva, *J. Solid State Electrochem.*, 2012, **16**, 3573-3580.
60. R. Shao, J. Niu, J. Liang, M. Liu, Z. Zhang, M. Dou, Y. Huang and F. Wang, *ACS Appl. Mater. Interfaces*, 2017, **9**, 42797-42805.
61. D. Q. Liu, Z. Jia and D. L. Wang, *Carbon*, 2016, **100**, 664-677.
62. X. J. Li, J. Zhou, W. Xing, F. Subhan, Y. Zhang, P. Bai, B. J. Xu, S. P. Zhuo, Q. Z. Xue and Z. F. Yan, *Electrochim. Acta*, 2016, **190**, 923-931.
63. X. Wang, C. X. Lu, H. F. Peng, X. Zhang, Z. K. Wang and G. K. Wang, *J. Power Sources*, 2016, **324**, 188-198.
64. C. Chen, D. F. Yu, G. Y. Zhao, B. S. Du, W. Tang, L. Sun, Y. Sun, F. Besenbacher and M. Yu, *Nano Energy*, 2016, **27**, 377-389.
65. L. Zhang, T. You, T. Zhou, X. Zhou and F. Xu, *ACS Appl. Mater. Interfaces*, 2016, **8**, 13918-13925.

66. J. Xu, Z. Tan, W. Zeng, G. Chen, S. Wu, Y. Zhao, K. Ni, Z. Tao, M. Ikram, H. Ji and Y. Zhu, *Adv. Mater.*, 2016, **28**, 5222-5228.
67. X. M. Fan, C. Yu, J. Yang, Z. Ling, C. Hu, M. D. Zhang and J. S. Qiu, *Adv. Energy Mater.*, 2015, **5**, 1401761-7.
68. Y. S. Yun, M. H. Park, S. J. Hong, M. E. Lee, Y. W. Park and H. J. Jin, *ACS Appl. Mater. Interfaces*, 2015, **7**, 3684-3690.
69. N. N. Guo, M. Li, X. K. Sun, F. Wang and R. Yang, *Green Chem.*, 2017, **19**, 2595-2602.

Table of Content:

